Nigerian Research Journal of Chemical Sciences (ISSN: 2682-6054)
Volume 14, Issue 1, 2026

Adsorption of Cadmium Ions Using Chemically Activated Palm Kernel Shell: Kinetic, Equilibrium and Thermodynamic Interpretations

[*1,2]Idowu J. Esho, [1]Emmanuel F. Olasehinde and [2]Matthew A. Adebayo

[1]Department of Chemistry, The Federal University of Technology, Akure, Nigeria.

[2]Department of Chemistry, Federal College of Education (Special), Oyo, Nigeria.

*Corresponding Author: esho.idowu2627@fcesoyo.edu.ng

Accepted: *March 3, 2026*. **Published Online***: March 13, 2026*

ABSTRACT

This study synthesised and evaluated chemically activated, pyrolysed palm kernel shell biochar (CPPKS) as a high performance adsorbent for Cd^{2+} removal from aqueous solutions, with detailed kinetic, equilibrium, and thermodynamic analyses. Palm kernel shells were pyrolysed and activated using H_3PO_4. Characterisation by Fourier Transform Infrared Spectroscopy (FTIR) for abundant oxygen-containing functional groups (–OH, C=O), Scanning Electron Microscope coupled with Energy Dispersive X-ray (SEM–EDX), X-ray Diffraction (XRD), Thermo-gravimetric Analysis (TGA) determine its structural, morphological, and surface properties, while Brunauer-Emmett-Teller (BET) surface area analysis confirmed a mesoporous structure (117.47 m^2/g; 3.46 nm; 1.240 cm^3/g), and zeta potential measurements indicated a point of zero charge (pHpzc) of 5.20, favouring adsorption at pH 6. Batch studies examined pH, contact time, concentration, dosage, and temperature effects. Avrami fractional-order model (R^2 = 0.99115) described kinetic data, while equilibrium followed the Liu isotherm ($R^2 \approx 0.99999$). Thermodynamic parameters ($\Delta G°$, from −2.34 to −5.71 kJ/mol; $\Delta H°$ = 23.28 kJ/mol; $\Delta S°$ = 86.96 J/mol K) showed a spontaneous, endothermic process with increased disorderliness. Adsorption involved electrostatic attraction, ion exchange, complexation, and diffusion. Optimisation, regeneration studies, real effluent testing, and pilot-scale validation are recommended.

Keywords: Avrami kinetics, Cd^{2+} adsorption, Liu isotherm, Palm kernel shell biochar, Thermodynamic study

INTRODUCTION

Contamination of aquatic environment by cadmium (Cd^{2+}) is a major environmental challenge and public health problem as a result of its toxicity, mobility, and bio-accumulative nature, and shows higher levels of toxicity even at low concentrations. The major industrial sources of Cd^{2+} are from

electroplating, battery manufacturing, and pigment production. Health issues such as renal dysfunction, bone demineralisation, and carcinogenic impacts resulting from the prolonged exposure [1, 2]. Particularly at low concentration, high cost of operation and generation of secondary pollutants are the frequent challenges encountered by traditional treatment methods, such as chemical precipitation, ion exchange, and membrane filtration, employed in remediating heavy metals [3].

The best method for remediating cadmium(II) ions from the environment is adsorption, which is eco-friendly, affordable, and cost-effective [4]. Due to high porous structure, enhanced surface chemistry, and higher surface area are achieved in activated biochar, which improve binding of heavy metal ions onto adsorbent surface, hence it is broadly applied [5]. Biochar produced by valorising agricultural wastes biomass has gained interest owing to the high cost of commercial activated carbon [6].

The abundance of palm kernel shell (PKS), as a by-product of the palm oil industry, is an attractive starting material for the production of activated carbon as a result of affordability, availability, and possession of high carbon residue [1, 7]. Chemical activation, using agents such as H_3PO_4, KOH, or $CaCl_2$, significantly enhances PKS-derived biochars by increasing surface area, pore volume, and functional group density [2]. Ling *et al.* [7] noted that high adsorption capacity of Cd^{2+} ions onto adsorbent surfaces *via* functional groups containing oxygen atom and formation of microporous and mesoporous networks.

In addition, for rationale adsorbent design, it is essential to have in-depth knowledge of the adsorption mechanisms of cadmium(II) ions on chemically activated palm kernel shell biomass. Surface precipitation, ion-exchange, electrostatic attraction, and surface complexation are required for increase adsorption of Cd^{2+} ions [7]. The surface charge and solution pH are critical: Cd^{2+} adsorption is favoured when the carbon surface is negatively charged relative to the metal cation [8]. Chemisorption mechanism is obtained from high contributions of oxygen-containing groups, which act as ligand sites, forming inner-sphere complexes [5].

Adsorption investigations indicate that the removal of Cd^{2+} on activated carbon derived from palm kernel shell frequently fits the isotherms from Langmuir or Freundlich, showing monolayer or heterogeneous multilayer adsorption depending on the chemistry on the surface [1]. Kinetic studies often follow pseudo-second-order models, indicating the importance of chemical interactions between the surface functional groups and Cd^{2+} ions [7].

As the investigation on adsorbents produced from palm kernel shell, knowledge gap still persists in linking cadmium(II) ions mechanisms at the molecular level and surface physicochemistry. Wipawee and Attaso [9] noted that to optimise chemical activation protocols, enhance performance of adsorption, and scale adsorbent produced from palm kernel shell for actual wastewater treatment applications, it is essential to describe these mechanisms. To bridge this significant knowledge gap, adsorption modelling and advanced characterisation employed so as to analyse the surface interactions and mechanistic pathways of Cd^{2+} adsorption on chemically activated palm kernel shell.

The study aimed at synthesizing and comprehensively evaluates chemically activated, pyrolysed palm kernel shell biochar as a high-performance adsorbent for Cd^{2+} removal from aqueous solution, with detailed kinetic, equilibrium, and thermodynamic analyses.

MATERIALS AND METHODS

All the reagents used were of analytical grade and used without further treatment. Phosphoric acid (H_3PO_4; CAS number: 7664-38-2), sodium hydroxide (CAS number: 1310-73-2), $Cd(NO_3)_2$ were obtained from Merck Chemical Company, Germany.

Sample Collection

Palm kernel Shells (PKSs) were collected from a palm oil deposit farmland at Ijimo village in Ilesa metropolis, Nigeria and authenticated at the Department of Crop, Soil and Pest Management, Federal University of Technology, Akure, Nigeria.

Valorisation of PKSs as Adsorbents and Characterization

The Raw Palm kernel Shells (RPKSs) were separated from stones and dirt, washed, and then pulverised to granules using industrial machine, and later ground in into powder with mortar and pestle continuously, sieved with 2 mm mesh size to obtain powder sample, and further converted to a fine powder using grinding stone. The powder sample was then stored in an air-tight container and labelled for further processing. Powdered RPKS (310 g) was weighed into 2 clay pot crucibles. The samples were introduced into a muffle furnace (Gallenkamp model) at 500 °C under nitrogen gas for 15 min, sieved with 106 μm mesh, and then stored in sealed plastic containers prior processing. A 200 mL of 1.0 M H_3PO_4 (activating agent) was mixed with 75 g of PPKS (one part of the sample). The mixture was agitated at 80 ºC (under reflux) for 4 h and was left for another

20 h for equilibration. After acid treatment, the mixture was washed with double distilled water several times until neutrality, dried in an oven at 105 ºC for 48 h, sieved with 106 µm mesh, and then stored in an air tight container until usage [9–11]. This adsorbent was labelled Chemically-Pyrolyzed Palm Kernel Chaff (CPPKC)

An FTIR spectroscopy (TENSOR 27, Bruker) was used to investigate the adsorbent's functional groups in a wavelength range of 4000 – 500cm^{-1} with a resolution of 8.0 cm^{-1}. The morphological properties and elemental composition of CPPKS were examined by Scanning Electron Microscopy (SEM, Hitachi SU 3500 scanning microscope, Tokyo, Japan) equipped with Energy Dispersive X-ray (EDX) spectrophotometer. The SEM images were taken at 500X magnification. Pore properties and BET (Brunauer-Emmett-Teller) surface areas were analysed using nitrogen adsorption-desorption isotherm at 80 K (ASAP2023 V4.02H, micrometrics, USA). For BET analysis, the samples were degassed at 437 K for 3 h. The thermal stability of the adsorbent samples was performed using thermogravimetric analysis (TGA; PerkinElmer Thermal Analyzer). Crystalline phases of the adsorbent were carried out by X-ray Diffraction spectrophotometer (Shimadzu XDS 2400H diffractometer). An electrokinetic analyser (Surpass 2, Anton Paar, Graz, Australia) was used to determine the zeta potential of the sample.

Batch Adsorption Studies, Modelling and Statistical Analysis

A stock solution of cadmium (1000 mg/L) was prepared by dissolving 2.75 g of $Cd(NO_3)_2$ in 1 L of distilled water. The working concentrations were generated *via* serial dilution. Adsorption experiments were carried out using a batch technique by adding 20 mL of the metal solution to a known mass (e.g. 0.05 g) of prepared activated adsorbents (CPPKS) in different 50 mL sample bottles. The pH (2, 4, 6, 8, 10) and contact time (2 – 480 min) effects on adsorption behaviours were investigated. The pH of the solution was adjusted using 0.5 M HCl and 0.5 M NaOH solutions. Initial concentration (50 – 800 mg/L), adsorbent dose (0.01 – 1.0 g), and temperature (25 – 60 °C) effects were investigated. The mixtures were stirred at 150 rpm on electrical thermostatic shaker and filtered to separate the spent adsorbents from un-adsorbed adsorbate in the solutions. The final solutions were then analysed for the residual cadmium(II) concentrations after adsorption using atomic absorption spectrophotometer (AAS; Perkin Elmer Analyst 700 model). The percentage (%) adsorption and the amount of cadmium(II) adsorbed at equilibrium (Q_e) were calculated from the data obtained using equations 1 and 2, respectively, [12, 13].

$$\%Adsorption = \frac{C_o - C_e}{C_o} \times 100 \quad [1]$$

$$Q_e = (C_o - C_e) \cdot V \cdot m^{-1} \quad [2]$$

where C_o = initial cadmium(II) concentration (mg/L), C_e = cadmium(II) concentration at equilibrium (mg/L), V = volume of the cadmium(II) solution used for the experiment (L), and m = mass of the adsorbent (g).

The time-dependent adsorption data were subjected to three non-linear kinetic models (pseudo-first order, pseudo-second order, and Avrami fractional) which are represented in equations 3 – 5, respectively, as well as intraparticle diffusion model (Equations 6). The isothermal data were subsequently analysed using non-linear forms of Langmuir, Freundlich, and Liu models, shown respectively in equations 7 – 9.

$$Q_t = Q_e \{1 - \exp(-k_1 t)\} \quad [3]$$

$$Q_t = \frac{Q_e^2 k_2 t}{k_2 Q_e t + 1} \quad [4]$$

$$Q_t = Q_e \left\{1 - \exp(-k_{Av} t)^{n_{Av}}\right\} \quad [5]$$

$$Q_t = k_{ipd} t^{0.5} + C \quad [6]$$

$$Q_e = \frac{Q_{\max} K_L C_e}{1 + (K_L C_e)} \quad [7]$$

$$Q_e = K_F C_e^{\frac{1}{nF}} \quad [8]$$

$$Q_e = \frac{q_{\max} (K_g \cdot C_e)^{n_g}}{1 + (K_g \cdot C_e)^{n_g}} \quad [9]$$

From the equations above, Q_t is the amount (mg) of the adsorbate (Cd^{2+}) adsorbed by 1 g of the adsorbents at a particular time, t; k_1 (min^{-1}) stands for the rate constant of pseudo-first order; k_2 (g mg^{-1} min^{-1}) denotes the rate constant for pseudo-second order; k_{AV} represents Avrami fractional order rate constant (min^{-1}); n_{AV} denotes the Avrami's fractional order, which is related to the mechanism of adsorption; k_{ipd} is the intraparticle diffusion rate constant (mg g^{-1} $min^{-0.5}$); C (mg g^{-1}) is the intraparticle diffusion constant, which is related to the thickness of the boundary layer; Q_{max} represents the adsorbent maximum adsorption capacity (mg g^{-1}); C_e is the equilibrium concentration of the chaff adsorbent (mg L^{-1}); K_L represents Langmuir equilibrium constant (L mg^{-1}); K_F denotes Freundlich equilibrium constant $\left((mg\ g^{-1})(mg\ L^{-1})^{-\frac{1}{nF}}\right)$; n_F is the Freundlich exponent; K_g denotes the rate constant for the Liu model (L mg^{-1}); and n_g is the adsorption intensity (dimensionless).

Equations 10 and 11 were used to calculate the values of the standard change in Gibb's free energy ($\Delta G°$, kJ mol^{-1}), standard change in enthalpy ($\Delta H°$, kJ mol^{-1}) and standard change in entropy ($\Delta S°$, J mol^{-1} K^{-1}) [13].

$$\Delta G^o = -RT\ln K \qquad [10]$$

$$\ln K = \frac{\Delta S^o}{R} - \frac{\Delta H^o}{RT} \qquad [11]$$

where R is the universal gas constant (8.314 J mol^{-1} K^{-1}), T is the temperature in Kelvin (K). The values of R^2_{adj} (adjusted determination coefficient) and χ^2_{red} (reduced chi square) of each model were used to determine the best model for the description of the adsorption data. The statistical expressions of R^2_{adj} and χ^2_{red} are represented in equations 12 and 13**,** respectively.

$$R^2_{adj} = \left\{1-(1-R^2)\right\}\left\{\frac{n-1}{n-p-1}\right\} \qquad [12]$$

$$\chi^2_{red} = \left\{\frac{1}{n-p}\right\}\sum_i^n \left(q_{i,\exp} - q_{i,\mathrm{model}}\right)^2 \qquad [13]$$

where n is the number of data points; p is the number of parameters in the model, $q_{i,model}$ and $q_{i,exp}$ are the individual data point predicted by model and obtained by experiment, respectively. A value

of R^2_{adj} close to one and very low value of χ^2_{red} signify excellent fit by a model [14, 15].

RESULTS AND DISCUSSION

The capacity of the prepared CPPKS of the adsorbent for removal of cadmium(II) from aqueous solutions were analysed using batch adsorption method.

Characteristics of the Adsorbents

The FTIR spectrum (Figure 1a) of the CPPKS demonstrates a complex surface chemistry characteristic of lignocellulosic-derived biochar. The broad peak at 3609 cm^{-1} (and the shoulder peak at 3202 cm^{-1}) is assigned to the O–H stretching vibrations of hydroxyl groups from phenols, alcohols, or adsorbed moisture, which are vital for surface hydrophilicity and strength of adsorption [16, 17]. The peak at 2763 cm^{-1} corresponds to C–H stretching in aldehydes or alkyl groups, while the sharp band at 2105 cm^{-1} indicates C≡C or C≡N triple bonds, frequently produced during carbonisation at elevated temperature [18]. The peak at 1781 cm^{-1} represents C=O stretching in carboxylic acids or lactones, indicating successful chemical activation or partial oxidation. Furthermore, the band at 1374 cm^{-1} is assigned to C–H bending in methyl groups, and the low-frequency peak at 632 cm^{-1} is a characteristic of C–H out-of-plane bending or mineral ash content. This functional profile confirms that the material possesses the requisite polar and non-polar sites for high-performance environmental applications, such as heavy metal removal or organic pollutant adsorption [18].

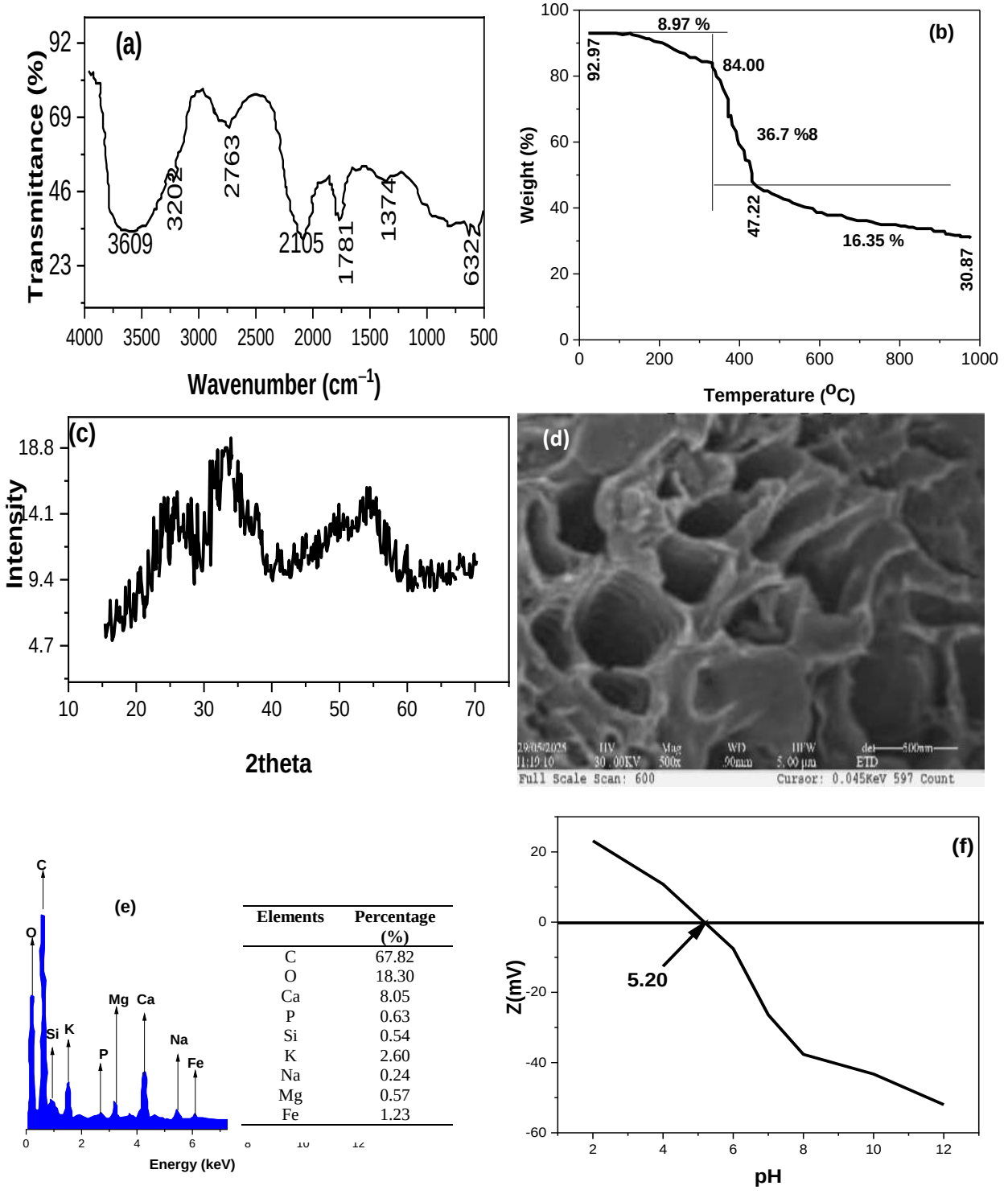

Elements	Percentage (%)
C	67.82
O	18.30
Ca	8.05
P	0.63
Si	0.54
K	2.60
Na	0.24
Mg	0.57
Fe	1.23

Figure 1: FTIR spectrum (**a**), TGA profile (**b**), SEM micrograph (**c**), XRD pattern (**d**), EDX spectrum and elemental composition (**d**), and Zeta potential (**e**) of the CPPKS

In Figure 1b (TGA profile) with clear distinct shifts, CPPKS demonstrates thermal breakdown in three stages of biomass that contains lignocellulosic materials. The initial stage occurred at about 180 °C with small loss of 8.97%, primarily attributed to the evaporation of surface-bound moisture and light volatiles, a value consistent with the moisture content reported for pre-treated oil palm residues in recent studies [19]. The shift point at 84% (weight loss) residue shows the beginning of breakdown of active lignin. The most aggressive stage representing devolatilisation at temperature 350 °C – 450 °C, demonstrates a major drop of 36.78% as cellulose and hemicellulose undergo rapid pyrolysis. The material stabilises with residue of 30.87% at temperature 1000 °C, indicating an overall improvement in thermal stability frequently obtained *via* phosphoric acid activation modification or carbonisation [20]. Therefore, it is evident that the carbon residue obtained at higher temperature confirms the adsorbent viable starting material for the production of activated carbon.

Figure 1c shows XRD pattern which substantiate a highly disordered amorphous network, a structural state highly prioritised in current investigation for high effective adsorption. The broad diffraction halo centered between 2θ of 20° and 35° illustrates the degradation of the tri-periodic crystalline structure of raw cellulose into a disordered carbon structure during thermochemical processing [21]. Yu *et al.* [22] reported that the dominance of this amorphous structure is not a structural deficiency but a functional asset; the lack of crystallinity aligns with higher defect amount and functional groups containing oxygen at the surface which act as primary binding sites for divalent heavy metal ions such as Cd^{2+} and Pb^{2+}. Present investigation on activated palm kernel shells shows that while the plane (002) showing rudimentary graphitic stacking, the overall structural looseness noted in this profile is pivotal for retaining the high microporous structure needed for accelerated diffusion kinetics in the treatment of wastewater [23].

Chemically activated pyrolysed palm kernel shell structural image (Figure 1d) shows an intense porous and irregular and surface architecture characterised by deep, well-defined cavities and honeycomb-like macro-pores. This morphological transformation is attributed to the aggressive degradation of the lignocellulosic matrix, specifically the removal of hemicellulose and lignin by chemical activating agents such as H_3PO_4 solutions [24]. Pitted topography formed shifts the raw biomass into a high-performance adsorbent by substantially elevating the pore volume and active surface area [25]. According to contemporary investigation, these structural voids are vital active sites for the storage of organic pollutants and heavy metals (Cd^{2+}), where the surface

roughness enhances the diffusion kinetics and physical binding of molecules within the framework of adsorbents [26].

EDX spectrum of the adsorbent (Figure 1e) illustrates chiefly framework rich in content, with carbon = 67.82% and oxygen = 18.30% as the major components. This major carbon structure, attribute of lignocellulosic biomass after pyrolysis or treatment with chemical, corresponds with similar investigations profiling palm kernel shell as a highly efficient feedstock for activated carbon and bio-composites owing to its intrinsic stability of lignin [27]. The presence of Ca, K, Mg with values 8.05%, 2.60%, and 0.57%, respectively, signifies a high amount of mineral ash, which contemporary research recognises as crucial for self-activation or catalytic functions in thermochemical transformation methods [28]. Additionally, the identification of micro constituents such as Fe = 1.23% and Si = 0.54% implies the capability of the material as a renewable adsorbent for removal of heavy metal removal and as a reinforcing agent in polymer structures, where these inorganic phases enhance stability in thermal and mechanical strength [29].

A pivotal parameter for determining the surface charge properties of adsorbents and thus their interaction mechanisms with ionic contaminants in aqueous media is zeta potential, while point of zero charge (*PZC*) is the charge at the solid surface of adsorbent determined by describes the mechanism of how adsorbate ions interact on protonation and deprotonation of adsorbate ions. The adsorbent zeta potential profile (Figure 1f) reveals a point of zero charge (pzc) of 5.20, indicating a shift from positively charged surfaces under acidic conditions to negatively charged surfaces at pH > 5.2. This behaviour is an attribute of chemically activated lignocellulosic biochar, where deprotonation of surface oxygenated functional groups improves electrostatic attraction toward cationic species (Pb^{2+}, Cd^{2+}) at near-neutral pH. Current investigations illustrate that tuning surface chemistry through chemical activation markedly reduces pHpzc and optimises the uptake of metal ion *via* integrated electrostatic interaction, complexation, and ion-exchange mechanisms [30]. pH above 6 shows a significant negative charge in the adsorbent which validates improved surface reactivity and stability, aligned with adsorbents from biochar documented for ecological friendly methods of removing heavy metal [31].

The BET data of CPPKS signify the capacity of the adsorbent as an efficient mesoporous material. The pore diameter of CPPKS is 3.4550 nm and this value categorises the material within the mesoporous range (2 – 50 nm) based on IUPAC classification, which is crucial for the diffusion and adsorption of larger molecular pollutants such as complexes formed from dyes and heavy

metal [32]. The BET surface area of the adsorbent is 117.465 m^2/g and this is moderately compared to highly activated carbons while the total pore volume of the adsorbent is 1.2400 cm^3/g. Moreover, the adoption of H_3PO_4 solution as a chemical activator is a current green chemistry inclination, which supports the formation of functional groups containing oxygen and preserves a resilient mesoporous structure at lower carbonisation temperatures, typically between 400 °C and 600 °C [33].

Adsorption Performances of RPKS and PPKS at varying pH Values

Figure 2a shows pH range of the adsorbent with the adsorption capacity peak at pH 6, a pattern confirmed by current studies where maximum amount of Cd^{2+} uptake generally manifests in the pH range of 5.0 to pH 6.5. At reduced pH, there is competition between the hydrogen ions and Cd^{2+} for active sites, while at pH values above 8, the development of precipitates of cadmium hydroxide, $Cd(OH)_2$, starts to control, resulting in a observed decline in actual adsorptive removal [34, 35].

Figure 2b shows dosage curve highlights substantial improvement in performance (15% to 95%) occurs when the dosage of the adsorbent is increased from 0.01 g to 0.06 g, after which a saturation point is attained. This effect of dosage is linked to the elevated availability of surface area and active functional groups, which are typical of chemically modified palm kernel shells [36].

Figure 2c highlights that while the percentage removal might reduce at high concentrations, the equilibrium adsorption capacity (Q_e) surges directly proportional with the initial concentration (C_o). The study implies that the driving force offered by the concentration gradient surpasses the mass transfer resistance, a behaviour uniformly simulated by the Langmuir or Freundlich isotherms in recent studies to describe monolayer or heterogeneous surface interactions [37].

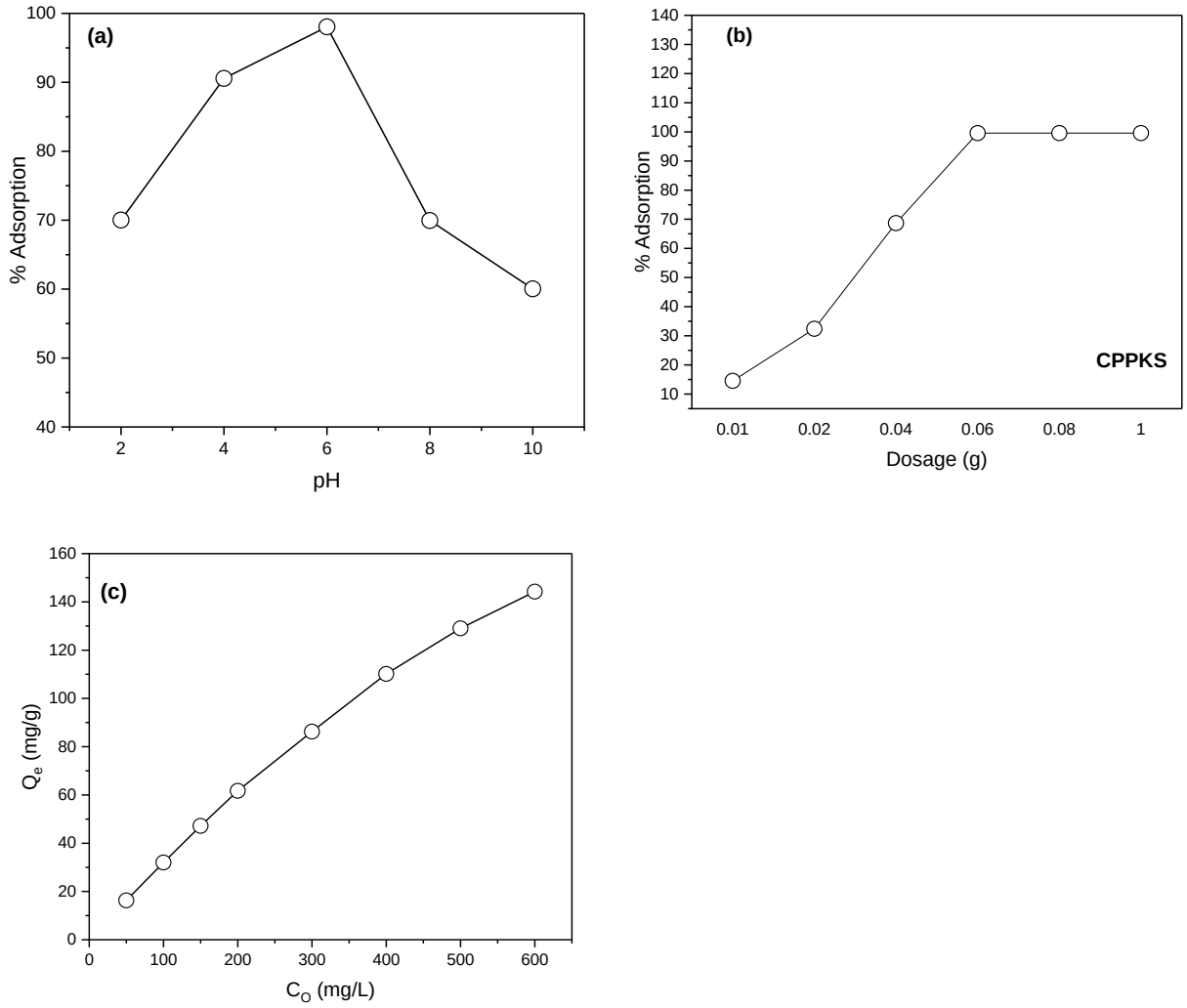

Figure 2: pH profiles (**a**), dosage profiles (**b**), and effect of initial concentration of Cd^{2+} (**c**) for adsorption of Cd^{2+} onto CPPKS

Kinetic Modelling of the Adsorption Process

Figure 3 and Table 1 present the respective kinetic profiles and parameters for adsorption of Cd^{2+} onto CPPKS. The profile in Figure 3a shows a fast early-stage adsorption followed by progressive strategy to equilibrium, suggesting a multiple step process controlled by external mass transfer and following interactions governed by the surface. The best fitting model for the kinetic data is Avrami fractional-order; this model offered the highest value of R^2_{adj} and lowest value of χ^2_{red} than other models and this observation corresponds to heterogeneous surface energetics and complex sorption routes [38].

The intraparticle diffusion profiles (Figure 3b) show that there are two stages (two linear sections) of adsorption process. The non-zero intercept in the intraparticle diffusion model further indicates that pore diffusion was not the major rate-limiting step. Such multi-mechanistic behaviour has been repeatedly documented for biochar and chemically activated agro-waste adsorbents in contemporary investigations, where chemisorption combined with diffusion-controlled transport controls Cd^{2+} uptake in mesoporous carbon frameworks [39].

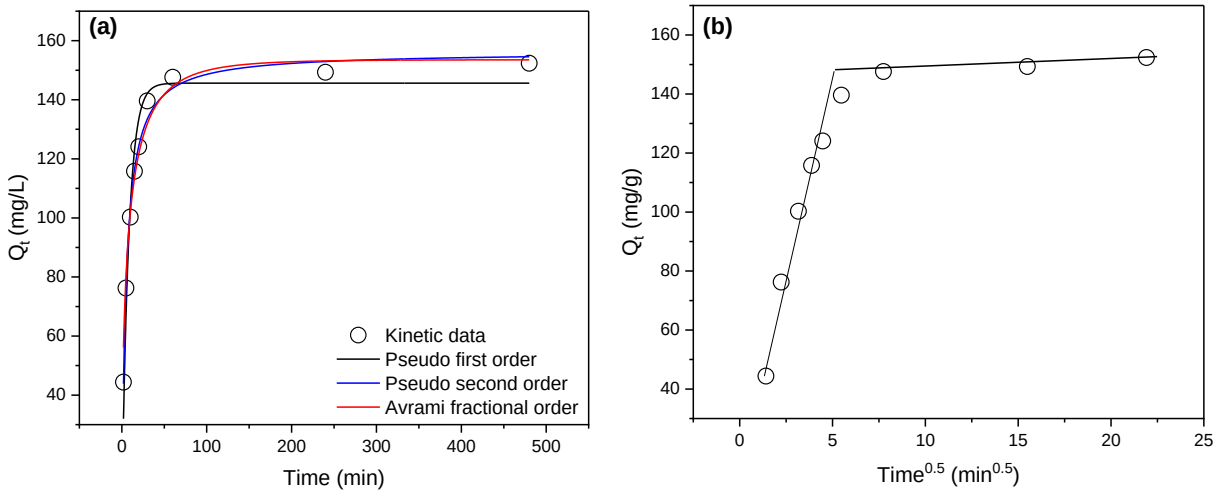

Figure 3: Kinetic (a) and intraparticle diffusion (b) profiles of CPPKC for adsorption of Cd^{2+}
Conditions: pH = 6; Dosage = 0.06 g; Agitation time: 2 – 480 min; Temperature= 25 °C

Table 1: Kinetic parameters for adsorption of Cd^{2+} onto CPPKS

Model	Parameters	Values
Pseudo-first order	$Q_{e,exp}$ (mg/g)	147.60
	$Q_{e,cal}$ (mg/g)	145.63
	k_1 (min^{-1})	0.12398
	R^2_{adj}	0.95879
	χ^2_{red} (mg/g)	64.793
Pseudo-second order	$Q_{e,cal}$ (mg/g)	156.22
	k_2 (g/mg min)	0.0012500
	R^2_{adj}	0.98268

	χ^2_{red} (mg/g)	11.502
Avrami fractional order	$Q_{e,cal}$ (mg/g)	153.55
	k_{AV} (min^{-1})	0.11581
	n_{AV}	0.53835
	R^2_{adj}	0.99115
	χ^2_{red} (mg/g)	1.3333
Intraparticle diffusion	k_{ipd} (mg/g $min^{0.5}$)	15.929
	R^2_{adj}	0.85530
	C (mg/g)	42.266

Equilibrium Description of the Adsorption Process

The equilibrium adsorption behaviour is mainly used to analyse the level of distribution of the adsorbates onto the surfaces of adsorbent. Langmuir, Freundlich, and Liu equilibrium models were used to elucidate the adsorption behaviour of Cd^{2+} ions onto the CPPKS adsorbents at different temperatures (25 – 60 ℃). Figure 4 and Table 2 represent the respective equilibrium curve (at 25 ℃) and parameters of the removal of Cd^{2+} by CPPKS. Liu isotherm, at times, performs best than the Langmuir and Freundlich models for adsorption of heavy metal on functionalised biochars because it simultaneously explains the surface energy heterogeneity and the saturation limit. The high (Q_{max}) values from Liu model presented in the table potentially indicate the mathematical sensitivity of the model to high-concentration data points instead of solely physical monolayer capacity, behaviour reported in contemporary studies regarding pseudo-saturation in highly porous adsorbents from agricultural waste [40]. The transition in (Q_{max}) between 40 ℃ and 60 ℃ is consistent with the recent observations on the thermal stability of metal-ligand complexes on cocoa-derived surfaces, where elevated temperature may induce desorptive kinetics or degradation of active structures [41].

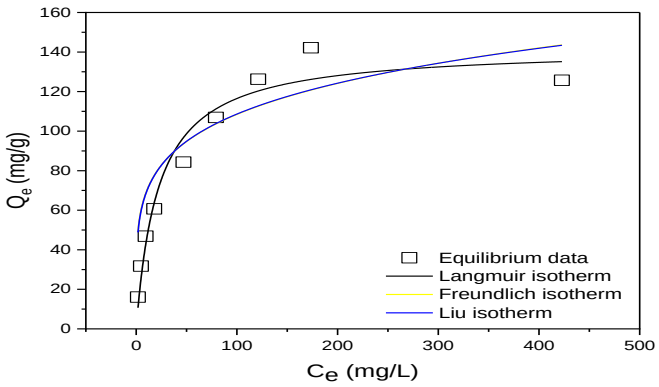

Figure 4: Equilibrium profile for the adsorption of cadmium(II)

Conditions: pH = 6; dosage = 0.06 g; agitation time = 2 h; Temperature= 25 ^{o}C; [Pb^{2+}] = 50 – 500 mg/L.

Table 2: Equilibrium parameters for adsorption of Cd^{2+} onto CPPKS

Model	Parameters	Values			
		25 ℃	40 ℃	50 ℃	60 ℃
Langmuir	Q_{max} (mg/g)	142.19	170.47	158.99	115.28
	K_L (L/mg)	0.022872	0.039868	0.052750	0.070038
	R^2_{adj}	0.96080	0.99032	0.83549	0.88636
	χ^2_{red} (mg/g)	93.399	26.934	262.46	161.03
Freundlich	$K_F\left((mg\ g^{-1})(mg\ L^{-1})^{-\frac{1}{n_F}}\right)$	44.229	18.349	5.2781	18.430
	n_F	5.1340	2.7376	2.0045	3.4346
	R^2_{adj}	0.87644	0.95472	0.76218	0.70067
	χ^2_{red} (mg/g)	58.815	126.03	379.41	424.20
Liu	Q_{max} (mg/g)	1722.8	10241	6724.5	4768.4
	K_g (L/mg)	0.022872	0.039868	0.052750	0.070038
	n_g	0.207780	0.36951	0.50460	0.29636
	R^2_{adj}	0.99996	0.99999	0.99999	0.99999
	χ^2_{red} (mg/g)	0.022452	0.0028979	0.0022379	0.0017106

Thermodynamic Characteristics of the Adsorption Process

Table 3 and Figure 5 show the thermodynamic parameters and van't Hoff's plot, respectively. The standard change in enthalpy ($\Delta H°$) and standard change in entropy ($\Delta S°$) were obtained by evaluating the temperature dependence of the equilibrium constant (K_g) through the van't Hoff equation (equation 11). A linear plot of ln K_g against $\frac{1}{T}$ was generated with R^2 value 0.99985, where $\Delta H°$ and $\Delta S°$ were calculated from the slope and intercept, respectively. The Gibb's free energy ($\Delta G°$) was calculated at each particular temperature using equation 10. In equations 10 and 11, K_g was substituted K and this represents the equilibrium adsorption constants of the Liu (best) isotherm fit. The values of K_g (L mg^{-1}) were converted to SI unit (m^3 mol^{-1}) (by multiplying with the molecular mass of the metal.

The parameters validating that spontaneous reaction occurs in the adsorption of Cd^{2+} onto CPPKS which is increasingly favoured at elevated temperatures, as demonstrated by the continuous negative values shown in standard Gibb's free energy change ($\Delta G°$) with values ranged from –2.3397 to –5.7128 kJ/dmol. The standard change in enthalpy ($\Delta H°$) is positive (23.279 kJ/mol) and this signifies an endothermic process controlled by ion-exchange mechanisms and surface complexation instead of weak physical adsorption, while the standard change in entropy ($\Delta S°$) showing positive potential with value of 86.964 J mol/K, indicates interfacial disorderliness owing to dehydration of Cd^{2+} during adsorption.

Table 3: Thermodynamic Parameters for Cd^{2+} for CPPKS

Temperature (K)	K_g (L/mg)	K_g (m^3/mol)	ΔG^o (kJ/mol)	ΔS^o (J/mol K)	ΔH^o (kJ/mol)	R^2
298	0.022872	2.5711	–2.3397	86.964	23.279	0.99985
313	0.039868	4.4817	–3.9034			
323	0.052750	5.9299	–4.7801			
333	0.070038	7.8733	–5.7128			

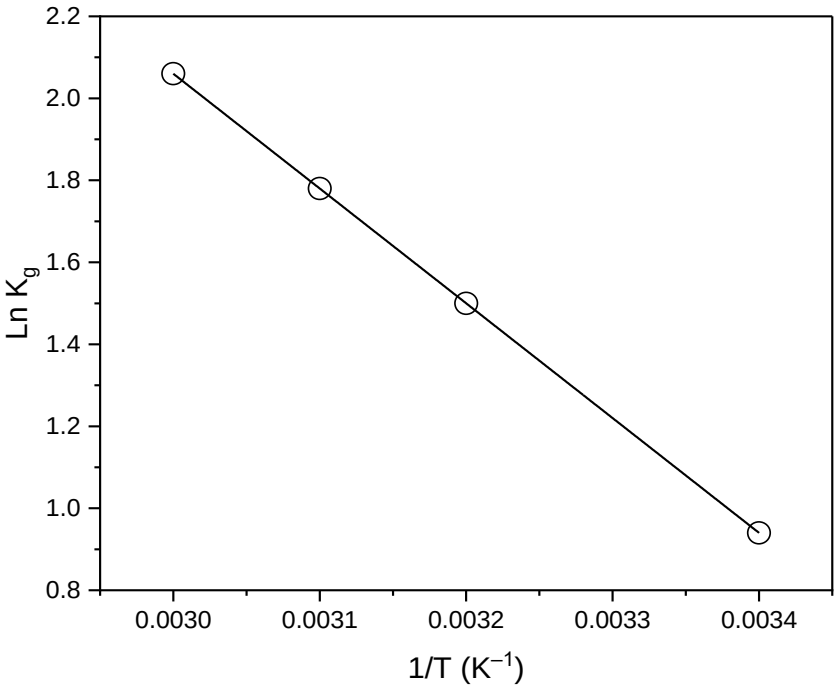

Figure 5: van't Hoff plot for adsorption of Cd^{2+} onto CPPKS

CONCLUSION

The present investigation quantitatively established that chemically-activated-pyrolysed palm kernel shell (CPPKS) is a structurally resilient and functionally active mesoporous bio-adsorbent for the removal of Cd^{2+} from water. FTIR examination validated high density oxygenated functional groups such as –OH at 3609 – 3202 cm^{-1}; C=O at 1781 cm^{-1}, while BET findings demonstrated a mesoporous diameter of 3.46 nm, pore volume of 1.240 cm^3/g, and surface area of 117.47 m^2/g, parameters aligned with adsorption improved by diffusion process. The confirmation of structural stability following activation is determined by thermal stabilisation up to temperature 1000 °C with carbon yield of 30.87%. The zeta potential value of 5.20 reinforces electrostatic favourability at near pH 7, where pH 6 showing maximum uptake of Cd^{2+}. Kinetic data fitted well to Avrami fractional-order model while the equilibrium data fitted best into Liu model. The highest (Q_{max}) values obtained at 40 °C from Liu model (10241 mg/g) shows the sensitivity of the model at high concentrations. Thermodynamic parameters ($\Delta G°$ = −2.34 to −5.71 kJ/mol; $\Delta H°$ = 23.28 kJ/mol; $\Delta S°$ = 86.96 J/mol K) support an entropy-controlled, spontaneous, endothermic adsorption process that is controlled by surface ion-exchange mechanisms and surface complexation

interactions. Overall, the results highlight CPPKS as a thermally stable, mesostructured, and mechanistically versatile adsorbent that are appropriate for heavy-metal remediation in wastewater systems through eco-friendly approach.

REFERENCES

1. Baby, R. & Hussein, M.Z. (2020). Ecofriendly approach for treatment of heavy-metal-contaminated water using activated carbon of kernel shell of oil palm. *Materials*, 13(11), 2627. https://doi.org/10.3390/ma13112627
2. Dechapanya, W. & Khamwichit, A. (2023). Biosorption of aqueous Pb(II) by H_3PO_4-activated biochar prepared from palm kernel shells (PKS). *Heliyon*, 9(7), e17250. https://doi.org/10.1016/j.heliyon.2023.e17250.
3. Baoying, W. Jingming, L., Chunmiao, B., Bolin, G. & Junjie, O. (2023). Adsorption of heavy metal onto biomass-derived activated carbon: review. *RSC Advances*, 13, 4275–4302. https://doi.org/10.1039/D2RA07911A.
4. Yichuan, M., Shuting, Z. & Jianlong, W. (2025). Adsorption of heavy metals by biochar in aqueous solution: A review. *Science of the Total Environment*, 968, 178898. https://doi.org/10.1016/j.scitotenv.2025.178898.
5. Muhammad, K., Muhammad, S., Junaid, R., Inas, A. Ahmed, A. Z., Katabathini, N. & Xiaohui, S. (2025). Mechanistic breakthroughs in affordable adsorbents for heavy metal remediation: An in-depth exploration of next-generation sustainable water purification technologies. *Journal of Hazardous Materials Advances*, 19, 100847. https://doi.org/10.1016/j.hazadv.2025.100847.
6. Sieng, H.K., Cerries, Y.J.C., Peter, N.Y.Y., Chee, C.W., Chee, S.W., Kah, Y.C., Rock, K.L. & Su, S.L. (2022). Removal of heavy metals using activated carbon from microwave steam activation of palm kernel shell. *Environmental Advances*, 9, 100272. https://doi.org/10.1016/j.envadv.2022.100272.
7. Ling, J., Gao, Y., Wang, R., Lu, S., Li, X., Liu, S. & Liu, J. (2025). Adsorption of Pb^{2+} and Cd2+ from Aqueous Solutions by Porous Carbon Foam Derived from Biomass Phenolic Resin. *International Journal of Molecular Sciences*, 26(15), 7302. https://doi.org/10.3390/ijms26157302.

8. Irshad, M. A., Younas, S., Nasim, I. Nawaz R., Amin Z. S., Perveen S., Khairy M., Irfan A., Al-Hussain S.A. Magdi E.A. & Zaki M. E. A., (2026). A comprehensive review of cadmium removal by adsorptive mechanism from wastewater using carbon-based nanotubes. *Applied Water Science*, 16, 20. https://doi.org/10.1007/s13201-025-02684-y
9. Wipawee D. & Attaso K., 2023. Biosorption of aqueous Pb(II) by H_3PO_4-activated biochar prepared from palm kernel shells (PKS). *Heliyon*, 9(7), e17250. https://doi.org/10.1016/j.heliyon.2023.e17250.
10. Barakat, N. A. M., Mahmoud, M. S. & Moustafa, H. M., 2024. Comparing specific capacitance in rice husk-derived activated carbon through phosphoric acid and potassium hydroxide activation order variations. *Scientific Reports*, 14, 1460. http://doi.org/10.1038/s41598-023-49675-0.
11. Gimba, C.E., J. Y., Olayemi, J. Y., Okunnu, S.T. & Kagbu. J. A., 2001. Adsorption of methylene blue by activated carbon from coconut shell. *Global Journal of Pure and Applied Sciences*, 7, 265–268.
12. Adebayo, M.A., Adediji, J.F., Adebayo, A.A. & Adebayo, O.T. (2012). Equilibrium, kinetic and thermodynamic parameters of the biosorption of Ni^{2+} from aqueous solution by *Streblus asper*. *Journal of Applied Sciences 12* (1), 71–77.
13. Olasehinde, E.F., Adegunloye, A.V., Adebayo, M.A. & Oshodi, A.A. (2018). Sequestration of aqueous lead (II) using modified and unmodified red onion skin. *Analytical Letters*, *51*(17), 2710–2732.
14. Aiyesanmi, A.F., Adebayo, M.A. & Fadairo, F.F. (2022). Evaluation of avocado pear seed coat for removal of nickel and chromium ions from aqueous solution. *Journal of Hazardous, Toxic, and Radioactive Waste*, 26(4): 04022027. https://doi.org/10.1016/10.1061/(ASCE)HZ.2153-5515.0000713
15. Aiyesanmi, A.F., Adebayo, M.A., Okoronkwo, A.E. & Ekujumi, O. (2022). Adsorption of Nickel (II) from Aqueous Solution Using Leucaena leucocephala Shells. *Iranian Journal of Chemistry and Chemical Engineering*, 41(8), 2755-2770.
16. Dai, F., Zhuang, Q., Huang, G., Deng, H. & Zhang, X. (2023). Infrared Spectrum Characteristics and Quantification of OH Groups in Coal. *ACS omega*, 8(19), 17064–17076. https://doi.org/10.1021/acsomega.3c01336

17. Boadu, K.O., Asiamah, I., Anang, A.M., John, K.B. & Wanjala, P.M. (2021). Characterization of chemically activated carbons produced from coconut and palm kernel shells using SEM and FTIR analyses. *American Journal of Applied Chemistry*, 9(3): 90–96. doi: 10.11648/j.ajac.20210903.15.
18. Sanni, O., Ren, J. & Jen T.C. (2024). Examining the ability of palm kernel shell extract to control corrosion and assess its economic value on thermo-mechanically treated steel in artificial seawater: a sustainable and environmentally friendly approach. *Frontiers in Chemistry*, 12, 1396565.
19. Hussain, M., Zabiri, H., Tufa, L. D., Yusup, S. & Ali, I. (2022). A kinetic study and thermal decomposition characteristics of palm kernel shell using model-fitting and model-free methods. *Biofuels*, 13(1), 105–116.
20. Ifeanyi, U., Emmanuel, O. & Momoh, S.A.A. (2022). Potentials of palm kernel shell derivatives: a critical review on waste recovery for environmental sustainability. *Cleaner Materials*, 6, 100154. https://doi.org/10.1016/j.clema.2022.100154
21. Hafizah, M.A.E., Manaf, A., Valency, T., Andreas, A. & Manawan, M. (2025). Optimized carbonization and kinetic analysis of palm kernel shell porous carbon for heavy metal adsorption. *Indonesian Journal of Chemistry*, 25(3), 787-799. https://doi.org/10.22146/ijc.100714
22. Yu, Y., He, J., Sun, J., Pei, Z., Wu, Q. & Yu, R. (2023). Capacity and Mechanisms of Pb(II) and Cd(II) Sorption on Five Plant-Based Biochars. *Sustainability*, 15(9), 7627. https://doi.org/10.3390/su15097627
23. Anto, S., Abdullah, M. E. & Meilana, D. P. (2022). Palm kernel shell activated carbon using phosphoric acid for crude palm oil clarification: properties and application. *Eur. Chem. Bull.*, 11(4), 1– 11.
24. Lawal, A., Muhammad, M.A., Hashim, T., Abbas, A. Y. & Halima, A. (2025). Palm Kernel Shell-Derived Nanoporous Carbon Materials: A Review on Preparation, Modification and Application. *The Caliphate Journal of Science and Technology* 1, 73–99. DOI: https://dx.doi.org/10.4314/cajost.v7i1.9.
25. Kopp, A.A., Hauschild, T., Basegio, T. M. & Berutti, F.A. (2024). Influence of lignin and cellulose from termite-processed biomass on biochar production and evaluation of chromium VI adsorption. *Scientific Reports*, 14, 14937. https://doi.org/10.1038/s41598-024-65959-5.
26. Aman, K., Monika, N., Nitin, K.S. & Sandeep, K. (2026). Recent progress and technological advancements for detection of micro/nano-plastics in the environment. *Advances in Colloid and Interface Science*, 351, 103817.

27. Tao, K.., Vladimir, S., Tim, E., Jing, H., Ravinder, K. & Qiang, L. (2020). Catalytic pyrolysis of lignocellulosic biomass: A review of variations in process factors and system structure. *Renewable and Sustainable Energy Reviews*, 134, 110305. https://doi.org/10.1016/j.rser.2020.110305
28. Wei, J., Tian, L., Sun, J., Ding, K., Li, B., Bai, Y., Rout, L., Liu, X., Xu, G. & Yu, G. (2024). Synergy effect of high K-low Ca-high Si biomass ash model system on syngas production and reactivity characteristics during petroleum coke steam gasification. *Energies*, 17(18), 4650. https://doi.org/10.3390/en17184650
29. Caixeta, A.L., da Silva, A.C.N. da Silva, S.K.S., Dias, M.C., Cholant, C.M., Volkmer, T. M., ... & Khan, S. (2025). Sustainable Biosorbent and Biopolymeric Materials for Heavy Metal Adsorption—Advances, Challenges, and Perspectives. *Materials*, *18*(20), 4752. https://doi.org/10.3390/ma18204752.
30. Macena, M., Pereira, H., Cruz-Lopes, L., Grosche, L. & Esteves, B. (2025). Competitive Adsorption of Metal Ions by Lignocellulosic Materials: A Review of Applications, Mechanisms and Influencing Factors. *Separations*, 12(3), 70. https://doi.org/10.3390/separations12030070
31. Hirpha, A.A., Abdisa, J., Melkiyas, D.M. &Abdi, N. E. (2024). Adsorptive performances and valorization of green synthesized biochar-based activated carbon from banana peel and corn cob composites for the abatement of Cr(VI) from synthetic solutions: Parameters, isotherms, and remediation studies. *Heliyon*, 10(13), e33811. https://doi.org/10.1016/j.heliyon.2024.e33811.
32. Khater, D., Alkhabbas, M., & Al-Ma'abreh, A.M. (2024). Adsorption of Pb, Cu, and Ni Ions on Activated Carbon Prepared from Oak Cupules: Kinetics and Thermodynamics Studies. *Molecules*, 29(11), 2489. https://doi.org/10.3390/molecules29112489
33. Yang, Z., Gleisner, R., H Mann, D., Xu, J., Jiang, J. & Zhu, J. Y. (2020). Lignin Based Activated Carbon Using H_3PO_4 Activation. *Polymers*, 12(12), 2829. https://doi.org/10.3390/polym12122829.
34. Qasem, N. A. A., Mohammed, R. H. & Lawal, D. U. (2021). Removal of heavy metal ions from wastewater: a comprehensive and critical review. *NPJ Clean Water*, 4, 36. https://doi.org/10.1038/s41545-021-00127-0
35. Aiyesanmi, A. F., Adebayo, M. A. & Fadairo, F.F. (2022). Evaluation of avocado pear seed coat for removal of nickel and chromium ions from aqueous solution. *Journal of Hazardous, Toxic, and Radioactive Waste*, *26*(4), 04022027.

36. Abiodun, O.-A. O., Oluwaseun, O., Oladayo, O.K., Abayomi, O., George, A.A., Opatola, E., Orah, R.F., Isukuru, E.J., Ede, I.C., Oluwayomi, O.T., Okolie, J.A. & Omotayo, I. A. (2023). Remediation of Heavy Metals Using Biomass-Based Adsorbents: Adsorption Kinetics and Isotherm Models. *Clean Technologies*, 5(3), 934–960. https://doi.org/10.3390/cleantechnol5030047
37. Gwadera, M., Brzoskwinia, P., Hnatyk, S. & Kazberuk, G. (2025). Mass Transfer Resistance Considerations for Dye Adsorption on Activated Carbon. *Purification*, 1(1), 4. https://doi.org/10.3390/purification1010004.
38. Zhou, D., Wei, J., Ge, L., Geng L., Zhou X., Lei L. L. (2025). Preparation and CO_2 adsorption of amino proton type ionic liquid @ KIT-6 composite material. *Journal of Materials Research* 40, 920–931. https://doi.org/10.1557/s43578-025-01546-2.
39. Wei, F., Jin, S., Yao, C., Wang, T., Zhu, S., Ma, Y., Qiao, H., Shan, L., Wang, R., Lian, X., Tong, X., Li, Y., Zhao, Q. & Song, W. (2023). Revealing the Combined Effect of Active Sites and Intra-Particle Diffusion on Adsorption Mechanism of Methylene Blue on Activated Red-Pulp Pomelo Peel Biochar. *Molecules*, 28(11), 4426. https://doi.org/10.3390/molecules28114426
40. Long, Z., Wang, Z., Huang, Q., Jia, Y., Jiao, Z., Wang, Y. & Du, Y. (2024). High-performance adsorption of methylene blue using novel bio-adsorbent based on *Sargassum fusiforme*. *Heliyon*, 10(18), e37949. https://doi.org/10.1016/j.heliyon.2024.e37949.
41. Răuță, D. I., Matei, E. & Avramescu, S.-M. (2025). Recent development of corrosion inhibitors: types, mechanisms, electrochemical behavior, efficiency, and environmental impact. *Technologies*, 13(3), 103.